# Development of the fragment-based COHSEX method for large and complex molecular systems

Takatoshi Fujita*
*Institute for Molecular Science, Okazaki, Aichi 444-0865, Japan*

Yoshifumi Noguchi
*Department of Applied Chemistry and Biochemical Engineering, Graduate School of Engineering, Shizuoka University, Hamamatsu, Shizuoka 432-8561, Japan*

(Received 1 October 2018; revised manuscript received 26 October 2018; published 20 November 2018)

We present a fragment-based many-body Green's function method suitable for treating large molecular systems in heterogeneous polarizable environments. The Green's function for a total system is approximated from fragment Green's functions and is expanded up to two-body terms. The screened Coulomb potential is approximated from the sum of intrafragment density-response functions, with interfragment polarization terms being neglected. The approximations for the Green's function and screened Coulomb potential lead to a many-body expansion of the self-energy. This expansion is essentially equivalent to the many-body expansion of the Fock matrix in the fragment molecular orbital method. To handle large molecular systems, the present implementation relies on the Coulomb hole plus screened exchange (COHSEX) approximation for the $GW$ self-energy. The accuracy of the FMO-COHSEX method was demonstrated in comparison to conventional COHSEX results for organic molecular aggregates. We confirmed that the present fragmentation approximation can provide reasonably accurate results, and mean absolute errors for quasiparticle energies of less than 0.1 eV have been achieved for valence orbitals. We also assessed the accuracy of the COHSEX approximation to describe the effects of molecular aggregation of electronic states, by comparing them with the $GW$ method. The COHSEX approximation has been shown to successfully describe the induced polarization and dispersion effects. As an illustrative application of the present method, we considered the electronic states of the pentacene thin film, which contains 1476 atoms. We investigated the impact of the induced polarization effect in the heterogeneous environment, highlighting the gap renormalization and the polarization-induced localization. This application shows that the present fragment-based method is useful for studying electronic structures of molecular aggregates in complex environments.

DOI: 10.1103/PhysRevB.98.205140

## I. INTRODUCTION

Organic electronics based on $\pi$-conjugated molecules or polymers have attracted considerable attention due to their features, such as their flexibility, light weight, and the tunability of electronic states. Due to their attractive characteristics, they have been utilized in a variety of electronic devices including field-effect transistors [1], light-emitting displays [2], and solar cells [3]. Many electronic processes governing the device operations occur at various interfaces. In a field-effect transistor, for example, charge carriers move near the surface of an organic semiconductor at the interface with a dielectric material. As known, dielectric materials considerably influence the behaviors of charge carriers [4–6]. In another example of an organic solar cell, charge separation processes occur at the electron-donor/electron-acceptor interfaces [7,8]. The choice of molecules, and the interfacial and bulk morphologies have significant effects on the electronically excited states formed at the interface [9,10]. Understanding the electronic states at the interfaces is essential to improve device efficiency and to rationally design novel materials.

Predicting electronic structures at the interfaces is still challenging because they depend on various factors. At the interfaces, the discontinuity of the electrostatic and polarizable environment alters the electronic levels [11,12]. Moreover, a static disorder of the molecular orbital (MO) energies is present because of the inherent structural disorder [13,14]. The structural disorder and heterogeneous polarizable environments lead to the localization of charge carriers or electronically excited states at the interfaces, which is in contrast to delocalized states in single crystals. The spatial extent of the wave functions are determined by the interplay between the electronic coupling and the disorder. Therefore the inclusion of both polarization and delocalization effects in complex environments is essential for simulations. Successful theoretical predictions of electronic structures at the interface require an advanced method, which goes beyond the framework of density functional theory (DFT) in general.

The $GW$ many-body Green's function approach has been established as an accurate and efficient method to predict electronic levels [15–18]. The neutral excitation and optical properties can also be treated in combination with the Bethe-Salpeter equation (BSE) approach [19,20]. The accuracy of the $GW$ and $GW$/BSE methods is well established by extensive benchmark studies against high-level quantum

*tfujita@ims.ac.jp

 

chemistry calculations [21–26]. The $GW$ method has widely been applied to organic systems, including isolated molecules [27–31], molecular solids [32–38], and single molecules adsorbed on surfaces [39–42]. The recent developments of efficient algorithms and parallel implementations have enabled the $GW$ calculations for systems over hundreds atoms [43–45]. It remains challenging, however, to treat more extended systems such as organic/organic interface systems.

Recently, Li *et al.* [46–48] have presented the hybrid quantum mechanics/molecular mechanics (QM/MM) approach based on the $GW$, which can be applied to complex molecular systems. They have employed the polarizable force field as the MM region, and the induced polarization from the MM region is incorporated as the reaction field Coulomb operator. However, the utilization of the convectional $GW$ method may restrict the system size in the QM region, which may imply that the charge delocalization effect is not fully considered. Therefore the earlier studies rely on the multiscale approaches [12,47,49], in which the charge delocalization effect is considered by transfer integrals in a tight-binding Hamiltonian.

In this manuscript, we present an implementation of the many-body Green's function method based on the fragment molecular orbital (FMO) method [50–52]. We introduce fragmentation approximations to calculate the Green's function and screened Coulomb potential, deriving the many-body expansion of the $GW$ self-energy matrix. The static Coulomb hole plus screened exchange (COHSEX) approximation of the $GW$ was employed to efficiently describe the polarization effect in large molecular systems. The advantage of this implementation is the consistent description of the electronic polarization and charge delocalization effects. We present benchmark calculations to validate the present implementation.

## II. THEORY

### A. Fragment molecular orbital method

First, we will briefly summarize the formulation of the FMO method [53]. The FMO is one of fragment-based electronic structure method that is suitable for treating large systems. In the FMO method, the total system is divided into many fragments, and the total energy is approximated from the energies of the fragment monomers, dimers, and optionally trimers. Although the FMO method was initially proposed as the many-body expansion of the total energy, the methods to approximate delocalized states of the total system, such as canonical MOs [54–57] and nonlocal excited states [58,59], have also been developed. More detailed theoretical formulations and applications of the FMO method have been reviewed elsewhere [50–52].

Within the two-body expansion of the FMO method, the self-consistent field (SCF) equations are solved for fragment monomers and fragment dimers,

$$F^X \left|\psi_p^X\right\rangle = \epsilon_p^X \left|\psi_p^X\right\rangle, \tag{1}$$

where $F^X$ is the fragment Fock operator and $X$ is $I$ for the fragment monomer or $IJ$ for the fragment dimer. Here, $|\psi_p^X\rangle$ and $\epsilon_p^X$ are the wave function and energy of the $p$th orbital, respectively. Because $F^X$ includes the electrostatic embedding potential from other fragments, the SCF equations for fragment monomers must be self-consistently solved until the charge densities of all fragment monomers converge. The SCF equations for the fragment dimers are then solved after the convergence of the monomer electron densities.

Next, we introduce the FMO-linear combination of molecular orbital (FMO-LCMO) method [55,60] to approximate canonical orbitals. Hereafter, we use a canonical orbital (CO) to refer to an eigenfunction of a one-body Hamiltonian of the total system. The fragment MOs obtained by Eq. (1) are localized within the fragment monomer or dimer, and the electron delocalization effect must be recovered to calculate the COs. Several methods [54–57] have been proposed to obtain COs from fragment MOs. The FMO-LCMO method introduced by Tsuneyuki *et al.* [55,60] adopts the many-body expansion of the Fock matrix,

$$\mathbf{F} = \sum_I \oplus \mathbf{F}^I + \sum_{I>J} \oplus (\mathbf{F}^{IJ} - \mathbf{F}^I \oplus \mathbf{F}^J). \tag{2}$$

The direct sum indicates that the elements of the fragment Fock matrices ($\mathbf{F}^X$) should be added to the total Fock matrix ($\mathbf{F}$) in the appropriate location. Diagonalization of the total Fock matrix as a generalized eigenvalue problem yields an approximate solution of the COs. In the FMO-LCMO method, the fragment Fock matrices are calculated in the basis of fragment monomer MOs. Because of this advantage, the dimension of the total Fock matrix can be efficiently reduced, for example, by considering several MOs near the HOMO-LUMO levels of the fragment monomers. In addition, the interfragment off-diagonal elements are equivalent to transfer integrals which can be used as charge-transfer couplings [61–63].

### B. Auxiliary basis and Cholesky decomposition

The present implementation is based on the real-space auxiliary basis function [27,64–66]. The resolution of identity, density fitting, or the Cholesky decomposition approach introduces an auxiliary basis function to represent pair products of atomic orbitals (AOs),

$$P(r) = \phi_\mu(r)\phi_\nu(r), \tag{3}$$

where $P(r)$ is an auxiliary basis, and $\phi_\mu$ and $\phi_\nu$ are Gaussian AOs. The four-center AO integral is approximately calculated from three- and two-center electron repulsion integrals:

$$(\mu\nu|\lambda\sigma) = \sum_{PQ} (\mu\nu|P) V_{PQ}^{-1} (Q|\lambda\sigma), \tag{4}$$

where $V_{PQ}^{-1}$ is the inverse matrix of the Coulomb operator represented in the auxiliary basis. In the $GW$ calculations, [66] the four-center MO integrals, $(pq|rs)$, appear when calculating the density response functions and self-energy. The four-center MO integrals are approximated as

$$(pq|rs) = \sum_P B_{pq}^P B_{rs}^P, \tag{5}$$

$$B_{pq}^P = \sum_{\mu\nu} C_{\mu p} C_{\nu q} (pq|Q) V_{QP}^{-\frac{1}{2}}. \tag{6}$$

Here, $C_{\mu p}$ represents the $p$th MO coefficients.

### C. Many-body expansion of the *GW* self-energy

In this section, we introduce the many-body expansion of the $GW$ self-energy. In the $GW$ approximation, the self-energy is calculated according to the following set of equations [15,16]:

$$\Sigma(r,r',\omega) = \frac{i}{2\pi}\int d\omega' G(r,r',\omega+\omega')W(r,r',\omega')e^{i\omega\eta}, \tag{7}$$

$$G(r,r',\omega) = \sum_p \left[\frac{\psi_p(r)\psi_p^*(r')}{\omega-\epsilon_p+i\eta sgn(\epsilon_p-E_F)}\right], \tag{8}$$

$$W(r,r',\omega) = v(r,r') + \int dr_1 dr_2 v(r,r_1)\chi(r_1,r_2,\omega)W(r_2,r',\omega), \tag{9}$$

where $G$ is the Green's function, $W$ is the screened Coulomb potential, $v$ is the bare Coulomb potential, $\chi$ is the noninteracting density-response function, $\eta$ is a positive infinitesimal, and $E_F$ is the Fermi level.

We aim to approximate the quantities above from the fragment MOs. Following the work by Yasuda and Yamaki [67], we adopted the cluster expansion of Green's function for the total system,

$$G = \sum_I G_I + \sum_{I>J}(G_{IJ} - G_I - G_J). \tag{10}$$

Here, the Green's function of fragment monomer or dimer is given as

$$G_X(r,r',\omega) = \sum_{p\in X}\left[\frac{\psi_p^X(r)\psi_p^{X*}(r')}{\omega-\epsilon_p+i\eta sgn(\epsilon_p-E_F)}\right]. \tag{11}$$

This cluster expansion is valid because each term represents the sum of the distinct diagrams.

Accordingly, the screened Coulomb potential is also approximated from the fragment MOs. In contrast to the fragment Green's function defined for the monomer or dimer, the screened Coulomb potential of the total system must be calculated because of the following consideration: when an electron is added to some fragment, the change in the fragment charge induces electronic polarization of the surrounding fragments. This induced electronic polarization cannot be treated by the screened Coulomb potential defined for fragment monomer or dimer. In the present study, the screened Coulomb potential of the total system is calculated from a sum of intrafragment density-response functions:

$$\chi(\omega) = \sum_I \chi^I(\omega), \tag{12}$$

$$\chi^I(\omega) = \sum_{\text{spins}}\sum_{i,a\in I}\left[\frac{\psi_i^{I*}(r)\psi_a^I(r)\psi_a^{I*}(r')\psi_i^I(r')}{\omega+\epsilon_a^I-\epsilon_i^I+i\eta} + \text{c.c.}\right]. \tag{13}$$

Here, $i$ and $a$ refer to the occupied and virtual MOs of the $I$th fragment, respectively. This approximation indicates that the interfragment polarization terms, the numerators of which are $\psi_i^{I*}(r)\psi_a^J(r)\psi_a^{J*}(r')\psi_i^I(r')$ $(I\neq J)$, can be neglected. Therefore this approximation is expected to work accurately for organic molecular aggregates, in which an electronic state is relatively localized within each molecule.

The approximations of the Green's function and screened Coulomb potential result in the many-body expansion of the self-energy,

$$\Sigma = \sum_I \Sigma^I + \sum_{I>J}(\Sigma^{IJ} - \Sigma^I - \Sigma^J), \tag{14}$$

where the fragment self-energy is defined as $\Sigma_X = iG_X \cdot W/2\pi$. This expansion is essentially equivalent to the many-body expansion of the Fock matrix [55,57] in the FMO. Note that the self-energies of fragment monomers and dimers are calculated using the same screened Coulomb potential. By considering the screened Coulomb potential of the total system, induced polarization effects of surrounding fragments can be included in the fragment self-energies. This treatment of the environmental potential goes beyond the conventional electrostatic embedding schemes.

A diagonal element, for example, is

$$\langle\psi_p^I|\Sigma|\psi_p^I\rangle = \langle\psi_p^I|\Sigma^I|\psi_p^I\rangle + \sum_{I>J}\left(\langle\psi_p^I|\Sigma^{IJ}|\psi_p^I\rangle - \langle\psi_p^I|\Sigma^I|\psi_p^I\rangle\right). \tag{15}$$

Here, the first term on the right-hand side of the equation is the monomer self-energy, and the second term is the dimer correction. In another example, the interfragment off-diagonal element $(I\neq J)$ is

$$\langle\psi_p^I|\Sigma|\psi_q^J\rangle = \langle\psi_p^I|\Sigma^{IJ}|\psi_q^J\rangle. \tag{16}$$

This term is the self-energy correction to the off-diagonal element in the Fock matrix.

### D. COHSEX approximation

In this section, we present working equations to evaluate fragment self-energy matrices within the COHSEX approximation [15,16]. The COHSEX is the static approximation of the $GW$ self-energy, which neglects the dynamical screening of the dielectric function. The COHSEX has been shown to overestimate the band gap in semiconductors [16]. However, because of its computational efficiency, the COHSEX approximation has been employed in the QM/MM approach [46,48], gradient calculations [68], and calculations of quasiparticle wave functions [25,69,70]. In this study, we employed the COHSEX approximation to treat large molecular systems, by assuming that the solid-state effects on the electronic structure can be reasonably described.

Within the COHSEX approximation, the fragment self-energy operator is decomposed as

$$\Sigma_{\text{COHSEX}}^X = V_{\text{HFX}}^X + \Sigma_{\text{SEX}}^X + \Sigma_{\text{COH}}^X, \tag{17}$$

where the $V_{\text{HFX}}^X$ is the Hartree-Fock (HF) exchange potential. The correlation part of the screened exchange (SEX) and the Coulomb-hole (COH) terms are given by

$$\Sigma_{\text{SEX}}^X = -\sum_i^{\text{occ}}\psi_i^X(r)\widetilde{W}(r,r')\psi_i^{X*}(r'), \tag{18}$$

$$\Sigma^X_{\mathrm{COH}} = \frac{1}{2}\sum_p \psi^X_p(r)\widetilde{W}(r,r')\psi^{X*}_p(r'), \tag{19}$$

where $\widetilde{W} = W - v$.

With the auxiliary functions and three-center integrals, the SEX and COH terms of the self-energy are calculated according to

$$\langle\psi^I_p|\Sigma^X_{\mathrm{SEX}}|\psi^J_q\rangle = -\sum_{i\in X}^{\mathrm{occ}}\sum_{PQ\in X} B^P_{pi}[(1-\Pi)^{-1}-1]_{PQ}B^Q_{qi}, \tag{20}$$

$$\langle\psi^I_p|\Sigma^X_{\mathrm{COH}}|\psi^J_q\rangle = \frac{1}{2}\sum_{r\in X}\sum_{PQ\in X} B^P_{pr}[(1-\Pi)^{-1}-1]_{PQ}B^Q_{qr}. \tag{21}$$

Here, $\Pi$ is the matrix representation of the density-response function for the total system in the basis of auxiliary functions; it is calculated as the sum of the intrafragment density-response functions, $\Pi = \sum_I \Pi^I$. The static limit of the intrafragment density-response function is

$$\Pi^I_{PQ} = 4\sum_{ia\in I} B^P_{ia}\frac{1}{\epsilon_i - \epsilon_a}B^Q_{ia}. \tag{22}$$

Here, we assumed a restricted HF or Korn-Sham (KS) method.

The COHSEX self-energy matrix for the total system is constructed according to Eq. (14). The quasiparticle Hamiltonian for the total system is defined by correcting the self-energy matrix (14) to the Fock matrix (2) in a perturbative manner,

$$H^{QP} = F + \Sigma - V_{\mathrm{XC}}, \tag{23}$$

where $V_{\mathrm{XC}}$ is the exchange-correlation potential (DFT) or the HF exchange potential (HF). As well as the FMO-LCMO Fock matrix, the self-energy matrix is calculated in the basis of fragment monomer MOs. Diagonalization of the quasiparticle Hamiltonian provides the approximate solutions of QP energies of the total system.

## III. IMPLEMENTATION

As described in Sec. II B, our implementation relies on the Gaussian AO basis and the auxiliary functions. Following the work of Blase *et al.* [27,65], we defined the auxiliary functions as a product of AOs belonging to the same atom. The auxiliary functions and three-center integrals were obtained from the Cholesky decomposition with adaptive metric (CDAM) introduced by Okiyama *et al.* [71]. In the CDAM method, the accuracy of the two-electron integrals is controlled by a decomposition threshold, and the number of the auxiliary basis is reduced by the prescreening process via a metric threshold [71]. According to the original work [71], the metric and decomposition thresholds were set to be $10^{-3}$ and $10^{-8}$, respectively.

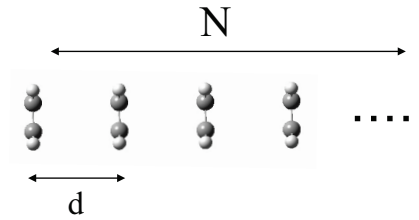


FIG. 1. The illustration of face-to-face one-dimensional molecular arrays.

The FMO-COHSEX calculations begin with a conventional FMO calculation. After the SCF equations for the fragment monomers, the intrafragment density-response functions are calculated from the monomer MOs. The screened Coulomb potential is then approximated from the sum of intrafragment density response functions, and the monomer self-energies are calculated from the monomer Green's functions and the screened Coulomb potential. Likewise, the dimer self-energy matrices are also calculated after the SCF equations of fragment dimer. The FMO-COHSEX method was implemented in the locally modified version of the ABINIT-MP program [51,72].

## IV. BENCHMARK CALCULATIONS

In this section, we report FMO-COHSEX benchmark results to validate the present implementation. The molecular systems considered as the benchmark are one-dimensional molecular arrays of ethylene (EHY), benzene (BEN), or thiophene (THI) molecules. Because we are interested in applications to organic electronic materials, face-to-face molecular arrays with a spacing of $d$ were employed as a model for $\pi$-$\pi$ stacked systems, as illustrated in Fig. 1. By comparing the FMO-COHSEX results with those without the fragmentation approximation, we show the dependence of the accuracy on a number of molecules and the intermolecular separation. Moreover, we assess the accuracy of the COHSEX approximation for describing the effect of molecular aggregation on the electronic structures, by comparing them with the $GW$ results.

All FMO calculations were performed with each molecule being assigned as a single independent fragment. The FMO-COHSEX calculations were performed with the B3LYP starting point and cc-pVDZ basis set. All of the FMO-COHSEX and conventional COHSEX calculations were performed using the ABINIT-MP program [51,72].

The remainder of this section is organized as follows. In Sec. IV A, we describe the accuracy of the approximated screened Coulomb potential in the FMO-COHSEX method. In Sec. IV B, we consider the accuracy of the canonical QP energies obtained using Eq. (23). In Sec. IV C, we discuss the use of the COHSEX approximation to describe the molecular aggregation effects.

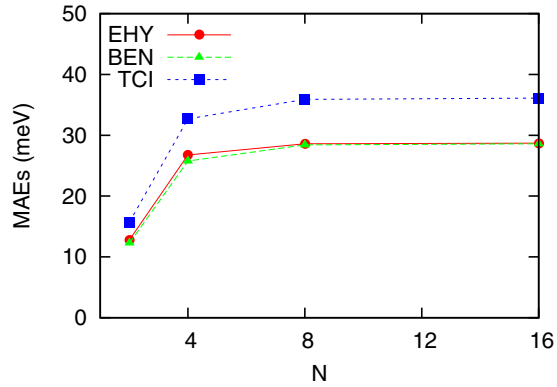


FIG. 2. Mean absolute errors (MAEs) of monomer QP energies with respect to the number of molecules in the molecular arrays.

TABLE I. Mean absolute errors of QPEs in units of meV, which were calculated for core, valence occupied, and virtual orbitals for one-dimensional molecular tetramers of EHY, BEN, or THI.

| | | $R = 3.0$ Å | 3.5 Å | 4.0 Å |
|---|---|---|---|---|
| EHY | Core | 175 | 97 | 48 |
| | Occ. | 55 | 52 | 29 |
| | Vir. | 63 | 49 | 25 |
| BEN | Core | 257 | 111 | 45 |
| | Occ. | 60 | 49 | 26 |
| | Vir. | 65 | 48 | 25 |
| THI | Core | 264 | 130 | 58 |
| | Occ. | 81 | 67 | 33 |
| | Vir. | 85 | 58 | 30 |

### A. Accuracy of the screened Coulomb potentials

The FMO-COHSEX method calculates the screened Coulomb potential from the sum of intrafragment density-response functions. This approximation assumes that the interfragment polarization terms and hybridization between MOs of different molecules are insignificant. In this part of the study, we investigated the accuracy of the approximation of the screened Coulomb potential.

To examine the approximation, we calculated monomer QP energies with an exact (without fragmentation) density-response function that was computed from the COs:

$$\chi_{\mathrm{CO}}(\omega=0) = 2\sum_{\mathrm{spins}}\sum_{i,a}\left[\frac{\psi_i^*(r)\psi_a(r)\psi_a^*(r')\psi_i(r')}{\epsilon_a-\epsilon_i}\right]. \quad (24)$$

In Eq. (24), $i$ and $a$ refer to occupied and virtual COs, respectively. Conventional DFT calculations were first performed to obtain the COs, and the screened Coulomb potential was calculated without the fragmentation approximation, $W_{\mathrm{ex.}} = v + v\cdot\chi_{\mathrm{CO}}\cdot W_{\mathrm{ex.}}$. The monomer self-energies with approximated screened Coulomb potential were compared with those with the exact screened potential, $\Sigma_I = iG_I\cdot W_{\mathrm{ex.}}/2\pi$.

The mean absolute errors (MAEs) for the monomer QP, relative to those with the exact screened potential, were calculated as averages of all monomer MOs. Figure 2 presents the MAEs of the monomer QP energies for one-dimensional EHY, BEN, and THI arrays with $d = 4.0$ Å. As shown in Fig. 2, the monomer QP energies with the exact screened potential are appropriately reproduced by the fragmentation approximation. Although the errors increase with increasing number of molecules, the MAEs are at most 25–35 meV for $N = 16$. We confirmed that for weakly interacting molecular systems, the approximation of the screened Coulomb potential is reasonably accurate.

We next turn to the case of stronger interactions. It is expected that the fragmentation approach can deteriorate when molecular interactions become stronger at shorter intermolecular separations. Here, molecular tetramers with $d = 3.0$, 3.5, and 4.0 Å were employed. To check the errors in more detail, the MAEs of monomer QP energies were separately averaged for core, valence occupied, and virtual orbitals. Table I shows the MAEs of the molecular tetramer at $d = 3.0$, 3.5, and 4.0 Å. As expected, the MAEs increases with decreasing the intermolecular separations. We found that the MAEs of the core orbitals are larger than those of the valence occupied and virtual orbitals. In addition, the MAEs of the core orbitals are considerably large at the shorter intermolecular separation; they are 97–130 meV at $d = 3.5$ Å and are 175–264 meV at $d = 3.0$ Å. However, the MAEs for the valence occupied and virtual orbitals are still marginal at shorter intermolecular separations; they are 55–85 meV at $d = 3.0$ Å and 48–67 meV at $d = 3.5$ Å. We conclude from the benchmark results that the screened Coulomb potential can be well approximated from the sum of the intrafragment density-response functions. Although the accuracy of the core orbitals requires further improvement, the present fragmentation approach can provide satisfactory results for valence orbitals even at shorter intermolecular separations.

### B. Accuracy of the canonical QP energies

In this section, we considered the accuracy of the FMO-COHSEX canonical QP energies. To investigate the accuracy of the canonical QP energies, the MAEs were averaged for $2N$ COs ($N$ highest occupied + $N$ lowest unoccupied COs). For the BEN arrays, the MAEs were averaged for $4N$ orbitals because of the two-degenerate HOMO and LUMO of the benzene molecule. Here, the FMO-LCMO Fock and self-energy matrices were constructed by collecting one HOMO and one LUMO for each molecule (HOMO-1 to LUMO+1 for BEN).

The accuracy of the canonical QP energies is determined by the approximated screened Coulomb potential and the fragmentation of the total Green's functions. The former determines the accuracy of the monomer QP energies, whereas the latter is associated with the self-energy corrections for interfragment interactions between monomer MOs. Figure 3 presents the MAEs of the canonical QP energies as a function of the number of molecules. The canonical QP energies are well reproduced by the FMO calculations, and the MAEs of the canonical QP energies fall in the similar range as those of the monomer QP energies. Therefore we confirmed that the FMO-COHSEX method can approximate

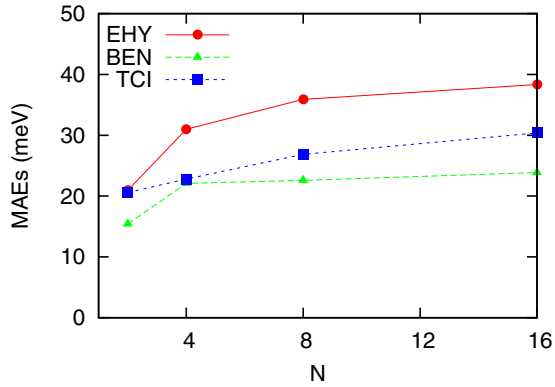


FIG. 3. Mean absolute errors (MAEs) of canonical QP energies with respect to the number of molecules in the molecular arrays.

the canonical QP energies of the total system with reasonable accuracy.

### C. Effects of dynamical screening

In this section, we explore the influence of the dynamical screening. Although the COHSEX approximation cannot quantitatively determine absolute QP energies [16,68,69], we are interested in the QP energy differences upon molecular aggregation. Therefore we assessed the validity of the COHSEX approximation for describing the effect of molecular aggregation on the electronic states.

Here, we consider the evolution of the highest occupied CO (HOCO) and lowest unoccupied CO (LUCO) upon increasing the number of molecules in the molecular arrays. We compared the COHSEX QP energies with those from the one-shot $GW$ ($G_0W_0$). The $G_0W_0$ calculations were performed using the FHI-AIMS software [66,73], in which the frequency dependence is treated by the imaginary frequency integration and analytical continuation. The effect of the molecular aggregation was investigated by calculating $\Delta\epsilon_p(N) = \epsilon_p(N) - \epsilon_p(N=1)$ ($p$ = HOCO or LUCO).

Figure 4 presents the $\Delta\epsilon_{\mathrm{HOCO}}(N)$ and $\Delta\epsilon_{\mathrm{LUCO}}$ for the 1D arrays of the BEN molecules. In general, the aggregation effects on the canonical QP energies are twofold: one is the effect of the induced polarization of surrounding molecules on the monomer QP energies. Another is the dispersion effect arising from the intermolecular orbital interactions. The overall trend of $\Delta\epsilon_p(N)$ is reproduced well within the COHSEX approximation, as indicated from the agreement between COHSEX and $G_0W_0$ shown in Fig. 4. Similar trends were also observed for the EHY and THI molecular arrays, as shown in Ref. [74]. Although the dynamical part of the $GW$ self-energy is essential for quantitative determination of QP energies, the COHSEX can accurately describe the effects of molecular aggregations.

The results encourage us to develop a hybrid approach, in which the dynamical part of the self-energy is evaluated for a target fragment with induced polarization of surrounding fragments being treated within the COHSEX. Indeed, a similar strategy has already been used in the aforementioned QM/MM $GW$ method [46,48], in which the polarization of the MM part was described within the static approximation.

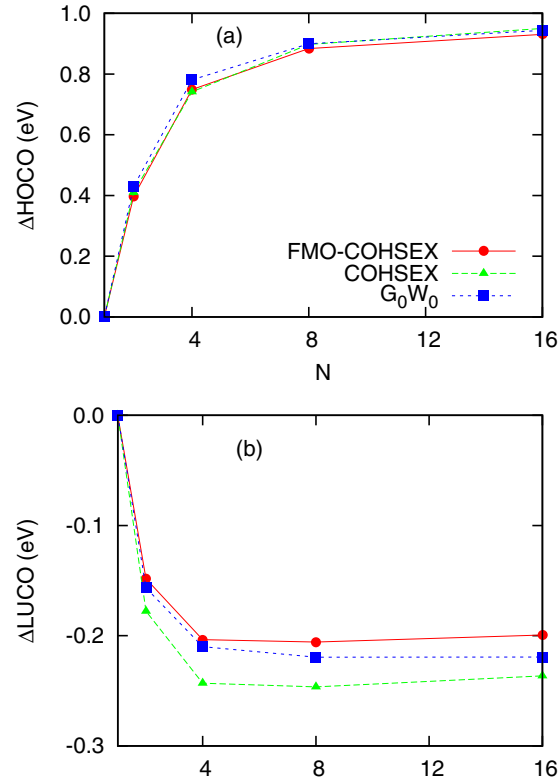


FIG. 4. The evolution of (a) HOCO and (b) LUCO QP energies with respect to the number of benzene molecules, which were obtained from the FMO-COHSEX, conventional COHSEX, and $G_0W_0$ methods.

Efficient treatment of the dynamical screening effect within the fragment-based method will be developed in a future study.

## V. APPLICATION TO THE PENTACENE THIN FILM

As an application of the FMO-COHSEX, we investigated the electronic level of a pentacene thin film. We employed the thin-film structure of pentacene crystal [77] (CCDC number: 665900). From the crystallographic information file, we prepared the thin-film structure containing 41 molecules, as depicted in Fig. 5. This system contains 1476 atoms and 5986 electrons. It is considered that the pentacene molecules in the thin-film structure are embedded in heterogeneous polarizable environments. The electronic states of molecules in the edge regions are similar to that of an isolated molecule, whereas those in the central region are more similar to bulk electronic states. Here, we discuss the polarization effects on the MO energies in Sec. V A and the spatial extent of the COs in Sec. V B.

The FMO-COHSEX calculation was performed using the B3LYP starting point with 6-31G* basis set. In the FMO calculation, the Mulliken point charge approximation [72] was adopted to calculate environmental electrostatic potentials; the electrostatic approximation for the separated fragment pairs was also employed with threshold values of 2.0 in van der Waals units [72]. The FMO-LCMO matrix elements for the

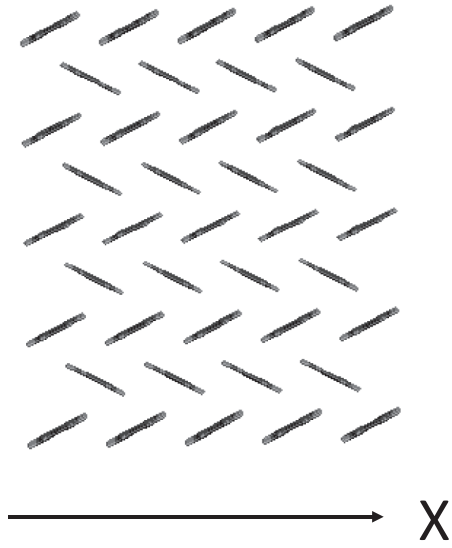


FIG. 5. The structure of pentacene thin film.

Fock and self-energy matrices were constructed using the HOMO and LUMO of each molecules.

### A. MO Energies in the thin-film structure

In this section, we discuss the HOMO and LUMO energies of single pentacene molecules in the thin-film structure. We start our discussion by presenting HOMO and LUMO energies of an isolated pentacene. COHSEX and B3LYP calculations were performed for an isolated pentacene molecule, the structure of which was optimized at the B3LYP/6-31G** level via GAUSSIAN software [78]. The HOMO/LUMO energies are $-7.070/-1.492$ eV according to COHSEX and are $-4.585/-2.495$ eV according to B3LYP. They lead to the COHSEX and B3LYP HOMO-LUMO gaps of 5.676 and 2.190 eV, respectively

Now, we turn to the MO energies in the thin-film structure. Here, the HOMO and LUMO energies in the thin film were obtained from the FMO matrix elements; the MO energies of B3LYP and COHSEX were calculated as diagonal elements of the total Fock matrix (2) and the total quasiparticle Hamiltonian matrix (23), respectively. The impact of the self-energy corrections on the MO energies can be clearly seen when the COHSEX HOMO-LUMO gaps are compared with those of B3LYP, as shown in Fig. 6. Remarkably, the B3LYP HOMO-LUMO gaps exhibit the small energy variation (2.261–2.279 eV). Moreover, the B3LYP gaps are slightly increased relative to the isolated one. In contrast, the COHSEX gaps exhibit the significant energy variation, and the standard deviation is as large as 0.332 eV. In addition, the COHSEX gaps in the thin film are significantly reduced relative to the isolated one. The variation in the COHSEX gaps reflects the heterogeneous polarizable environment in the thin-film structure. As shown in Fig. 6, the HOMO-LUMO gaps in edge regions are similar to that of the isolated pentacene, whereas those in the central region are decreased.

To gain deeper insight into the gap renormalization, the HOMO and LUMO energies were compared for the COHSEX and B3LYP, as presented in Fig. 7. To consider the effects

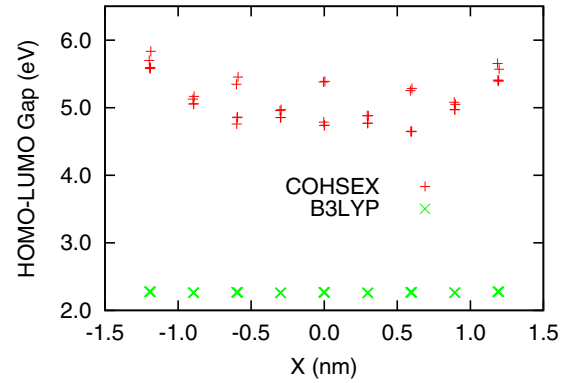


FIG. 6. HOMO-LUMO gap of each molecule in the pentacene thin film.

of the thin-film environment, the energy shift relative to the isolated one, $\epsilon_p^I - \epsilon_p^{\text{iso.}}$, was averaged for 41 pentacene molecules. The average HOMO/LUMO shifts are 0.572/0.115 eV for the COHSEX and are 0.478/0.401 eV for the B3LYP. The B3LYP energy shifts are due to the electrostatic effects dominantly arising from the pentacene quadrupole moments, while the COHSEX shifts also include the induced polarization effects of the surrounding molecules. The electrostatics have similar effects on the HOMO and LUMO energies if their spatial distributions are similar, and the B3LYP HOMO-LUMO gaps in the thin film are slightly increased by approximately 0.07 eV. In contrast, the induced polarization effects

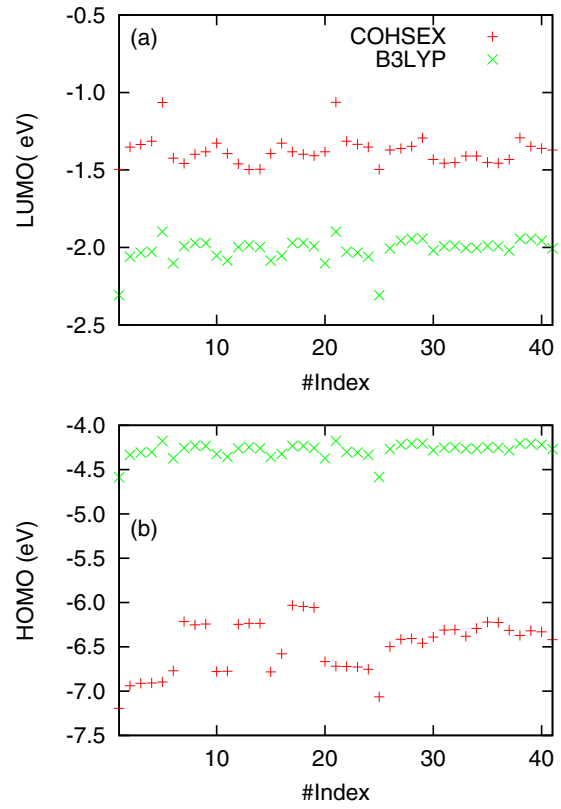


FIG. 7. HOMO and LUMO energies of each molecule in the pentacene thin film.

included in the self-energy correction tend to reduce the HOMO-LUMO gaps. The addition of an electron or hole induces the polarization of the surrounding molecules, creating an image charge to stabilize the anion or cation. Thereby, the electron in the HOMO/LUMO becomes destablized/stablized by the addition of the hole/electron, resulting in the reduction of the HOMO-LUMO gap [39–42].

We found that the increased variation in HOMO-LUMO gaps is due to the SEX contributions in the self-energy. As shown in the supplemental material, the variations in the COH contributions are similar for HOMOs and LUMOs, and the HOMO-LUMO gap shifts by COH are almost identical for all molecules. In contrast, the SEX terms of HOMOs show significant variation (6.47–7.30 eV), whereas those of LUMOs are less than 0.06 eV. Thus the SEX contribution is responsible for the increased variation in the HOMO-LUMO gap.

### B. Polarization-induced localization

Having investigated the MO energies, we next turn to the COs of the thin film and focus on the spatial extent of the wave functions. The solution of generalized eigenvalues problems of Eq. (23) yielded the canonical QP states, leading to 41 highest occupied and 41 lowest COs in the pentacene thin film. By omitting the negligible occupied-virtual block in the one-body Hamiltonian, the occupied and virtual COs were written as the superposition of the HOMOs and LUMOs of pentacene molecules, respectively, ($|\psi\rangle = \sum_I C_I |\psi_p^I\rangle$). Hereafter, we refer to HOMO-derived and LUMO-derived states as valence band (VB) and conduction band (CB) states, respectively.

We introduce the inverse participation ratio (IPR) to quantify the spatial extent of the wave function. The IPRs were calculated from the LCMO coefficients:

$$\mathrm{IPR} = \frac{1}{\sum_I |C_I|^4}. \tag{25}$$

The IPR defined by Eq. (25) denotes the number of molecules in which the wave function is delocalized. Figure 8 presents the IPRs of the VB and CB states. On one hand, the IPRs of the CB states are similar for the B3LYP and COHSEX. On the other hand, the IPRs of the VB states significantly change between the B3LYP and COHSEX. The self-energy corrections tend to decrease the spatial extent of the VB states. In general, IPRs become decreased for large variation in composite MO energies and for large electronic coupling elements among the MOs. As presented in the Supplementary Material, we found that the self-energy corrections of the off-diagonal elements are small. Therefore the lowering of the VB IPRs is due to the increased variation in HOMO energies as a result of the self-energy corrections. The induced polarization in the heterogeneous environment localizes the VB wave functions.

According to the FMO-COHSEX results, the self-energy correction has a minor effect on off-diagonal elements, which correspond to the transfer integrals. Therefore the localization of VB states was solely induced by the increased variation in the HOMO energies. However, this picture may contradict the earlier study by Busset *et al.* [79] who examined the

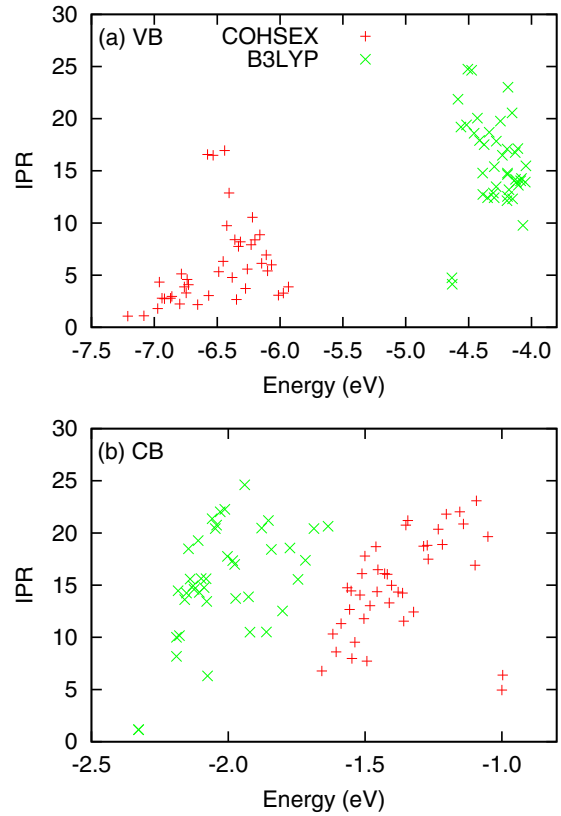


FIG. 8. Inverse participation ratio (IPR) of (a) VB and (b) CB states of the pentacene thin film, which were obtained from the FMO-COHSEX and FMO-B3LYP calculations.

polarization effect on electronic states. By employing a model Hamiltonian of a single charge carrier interacting with a quantum field of Frenkel excitons, they have shown that the transfer integrals in organic crystals are renormalized by the Frenkel exciton field. The ratio of renormalized and bare transfer integrals was estimated to be 0.64 in the pentacene crystal. In contrast, the corresponding ratios in this study (see Ref. [74] for details) are 1.05–1.08 and 1.00–1.05 for LUMO-LUMO and HOMO-HOMO transfer integrals, respectively. One possible reason for the disagreement is that the $GW$ method calculates the dielectric function at the random phase approximation (RPA) level, and the dielectric function beyond RPA may be necessary to renormalize the transfer integrals. The connection between the fragment-based Green's function method and their model remains to be elucidated.

## VI. CONCLUSION

In this paper, we have presented the implementation of the many-body Green's function method based on the FMO method. The present fragmentation approach adopts the many-body expansion of the Green's function, while the screened Coulomb potential is approximated from the sum of the intrafragment density-response functions. We have employed the COHSEX approximation to treat large molecular systems. The benchmark calculations were performed to numerically evaluate the accuracy of the fragmentation approximation. We found that MAEs of less than 0.1 eV are achieved

for valence orbitals, confirming that the FMO-COHSEX is satisfactory accurate for organic molecular aggregates. In addition, by comparing COHSEX with $G_0W_0$, we found that the COHSEX approximation can reasonably describe the molecular aggregation effects on electronic states, such as induced polarization and dispersion effects.

We note that the convergence of $GW$ quasiparticle energies in a Gaussian basis is very slow [22,80–82]. The accuracy of 0.1 eV compared to the complete basis set limit is reached at the level of the cc-pV5Z basis set [82]. However, it is unfeasible to use sufficiently large basis sets for large-scale calculations. In addition, the use of larger basis set decreases the accuracy in an FMO calculation [57,83], because it increases the overlap between basis functions and thus electronic couplings among fragments. The basis set size effect on the accuracy of the screened Coulomb potential will be assessed in a future study. Although the quantitative estimation of quasiparticle energies is challenging for large systems, the qualitative trends regarding the induced polarization effects can be investigated by the present fragment-based method with double-zeta quality basis sets.

We applied this FMO-COHSEX method to the pentacene thin film, which contains 1467 atoms. The present method has successfully described the gap renormalization of the pentacene molecules, whereas it is not possible using the conventional DFT. In addition, the variation in the HOMO-LUMO gaps was significantly increased by the self-energy correction, which reflects the heterogeneous polarizable environments of the thin-film structure. The application study confirmed that the FMO-COHSEX is useful for exploring electronic states of large molecular systems (over 1000 atoms) in complex environments. In addition, the advantage of our implementation is the consistent description of both polarization and delocalization effects. On account of the advantages, the present fragment-based Green's function method can become a powerful tool to treat organic electronic systems, in which the spatial extent of the electronic state at the interfaces plays an important role in the device operation.

## ACKNOWLEDGMENTS

T.F. thanks the financial support by Building of Consortia for the Development of Human Resources in Science and Technology, MEXT, Japan. T.F also thanks Dr. Yoshio Okiyama and Dr. Tatsuya Nakano at the National Institute of Health Science for providing the CDAM module. Y. N. acknowledges Grant-in-Aid for Scientific Research (C) (17K05565) from the Japan Society for the Promotion of Science (JSPS). The part of calculations in this manuscript was done using the facilities of the Supercomputer Center, the Institute for Solid State Physics, the University of Tokyo.

[1] H. Klauk, Chem. Soc. Rev. **39**, 2643 (2010).
[2] A. C. Grimsdale, K. Leok Chan, R. E. Martin, P. G. Jokisz, and A. B. Holmes, Chem. Rev. **109**, 897 (2009).
[3] A. Mishra and P. Bäuerle, Angew. Chem. Int. Ed. **51**, 2020 (2012).
[4] I. Hulea, S. Fratini, H. Xie, C. Mulder, N. Iossad, G. Rastelli, S. Ciuchi, and A. Morpurgo, Nat. Mater. **5**, 982 (2006).
[5] H. Matsui, A. S. Mishchenko, and T. Hasegawa, Phys. Rev. Lett. **104**, 056602 (2010).
[6] A. Laudari and S. Guha, J. Appl. Phys. **117**, 105501 (2015).
[7] T. M. Clarke and J. R. Durrant, Chem. Rev. **110**, 6736 (2010).
[8] F. Gao and O. Inganas, Phys. Chem. Chem. Phys. **16**, 20291 (2014).
[9] K. Vandewal, Annu. Rev. Phys. Chem. **67**, 113 (2016).
[10] Y. L. Lin, M. A. Fusella, and B. P. Rand, Adv. Energy Mater. **8**, 1702816 (2018).
[11] H. Houili, J. D. Picon, L. Zuppiroli, and M. N. Bussac, J. Appl. Phys. **100**, 023702 (2006).
[12] F. Castet, G. D'Avino, L. Muccioli, J. Cornil, and D. Beljonne, Phys. Chem. Chem. Phys. **16**, 20279 (2014).
[13] Y.-T. Fu, C. Risko, and J.-L. Brédas, Adv. Mater. **25**, 878 (2013).
[14] G. D'Avino, S. Mothy, L. Muccioli, C. Zannoni, L. Wang, J. Cornil, D. Beljonne, and F. Castet, J. Phys. Chem. C **117**, 12981 (2013).
[15] L. Hedin, Phys. Rev. **139**, A796 (1965).
[16] M. S. Hybertsen and S. G. Louie, Phys. Rev. B **34**, 5390 (1986).
[17] F. Aryasetiawan and O. Gunnarsson, Rep. Prog. Phys. **61**, 237 (1998).
[18] G. Onida, L. Reining, and A. Rubio, Rev. Mod. Phys. **74**, 601 (2002).
[19] G. Strinati, La Rivista del Nuovo Cimento **11**, 1 (1988).
[20] M. Rohlfing and S. G. Louie, Phys. Rev. B **62**, 4927 (2000).
[21] M. J. van Setten, F. Caruso, S. Sharifzadeh, X. Ren, M. Scheffler, F. Liu, J. Lischner, L. Lin, J. R. Deslippe, S. G. Louie *et al.*, J. Chem. Theory Comput. **11**, 5665 (2015).
[22] D. Jacquemin, I. Duchemin, and X. Blase, J. Chem. Theory Comput. **11**, 3290 (2015).
[23] F. Caruso, M. Dauth, M. J. van Setten, and P. Rinke, J. Chem. Theory Comput. **12**, 5076 (2016).
[24] T. Rangel, S. M. Hamed, F. Bruneval, and J. B. Neaton, J. Chem. Theory Comput. **12**, 2834 (2016).
[25] J. W. Knight, X. Wang, L. Gallandi, O. Dolgounitcheva, X. Ren, J. V. Ortiz, P. Rinke, T. Körzdörfer, and N. Marom, J. Chem. Theory Comput. **12**, 615 (2016).
[26] D. Jacquemin, I. Duchemin, and X. Blase, J. Phys. Chem. Lett. **8**, 1524 (2017).
[27] X. Blase, C. Attaccalite, and V. Olevano, Phys. Rev. B **83**, 115103 (2011).
[28] X. Blase and C. Attaccalite, Appl. Phys. Lett. **99**, 171909 (2011).
[29] Y. Noguchi, M. Hiyama, H. Akiyama, and N. Koga, J. Chem. Phys. **141**, 044309 (2014).
[30] Y. Noguchi and O. Sugino, J. Chem. Phys. **146**, 144304 (2017).
[31] Y. Noguchi and O. Sugino, J. Phys. Chem. C **121**, 20687 (2017).
[32] M. L. Tiago, J. E. Northrup, and S. G. Louie, Phys. Rev. B **67**, 115212 (2003).
[33] S. Yanagisawa, Y. Morikawa, and A. Schindlmayr, Phys. Rev. B **88**, 115438 (2013).
[34] S. Sharifzadeh, P. Darancet, L. Kronik, and J. B. Neaton, J. Phys. Chem. Lett. **4**, 2197 (2013).

[35] S. Sharifzadeh, C. Y. Wong, H. Wu, B. L. Cotts, L. Kronik, N. S. Ginsberg, and J. B. Neaton, Adv. Funct. Mater. **25**, 2038 (2015).

[36] T. Rangel, K. Berland, S. Sharifzadeh, F. Brown-Altvater, K. Lee, P. Hyldgaard, L. Kronik, and J. B. Neaton, Phys. Rev. B **93**, 115206 (2016).

[37] X. Leng, J. Feng, T. Chen, C. Liu, and Y. Ma, Phys. Chem. Chem. Phys. **18**, 30777 (2016).

[38] Y. Kang, S. H. Jeon, Y. Cho, and S. Han, Phys. Rev. B **93**, 035131 (2016).

[39] J. B. Neaton, M. S. Hybertsen, and S. G. Louie, Phys. Rev. Lett. **97**, 216405 (2006).

[40] K. S. Thygesen and A. Rubio, Phys. Rev. Lett. **102**, 046802 (2009).

[41] J. M. Garcia-Lastra, C. Rostgaard, A. Rubio, and K. S. Thygesen, Phys. Rev. B **80**, 245427 (2009).

[42] F. Marsusi, I. A. Fedorov, and S. Gerivani, J. Phys.: Condens. Matter **30**, 035002 (2018).

[43] D. Neuhauser, Y. Gao, C. Arntsen, C. Karshenas, E. Rabani, and R. Baer, Phys. Rev. Lett. **113**, 076402 (2014).

[44] M. Govoni and G. Galli, J. Chem. Theory Comput. **11**, 2680 (2015).

[45] W. Gao, W. Xia, X. Gao, and P. Zhang, Sci. Rep. **6**, 36849 (2016).

[46] J. Li, G. D'Avino, I. Duchemin, D. Beljonne, and X. Blase, J. Phys. Chem. Lett. **7**, 2814 (2016).

[47] J. Li, G. D'Avino, A. Pershin, D. Jacquemin, I. Duchemin, D. Beljonne, and X. Blase, Phys. Rev. Materials **1**, 025602 (2017).

[48] J. Li, G. D'Avino, I. Duchemin, D. Beljonne, and X. Blase, Phys. Rev. B **97**, 035108 (2018).

[49] G. D'Avino, L. Muccioli, Y. Olivier, and D. Beljonne, J. Phys. Chem. Lett. **7**, 536 (2016).

[50] D. G. Fedorov and K. Kitaura (eds.), *The Fragment Molecular Orbital Method: Practical Applications to Large Molecular Systems* (CRC Press, Boca Raton, FL, 2009).

[51] S. Tanaka, Y. Mochizuki, Y. Komeiji, Y. Okiyama, and K. Fukuzawa, Phys. Chem. Chem. Phys. **16**, 10310 (2014).

[52] D. G. Fedorov, WIREs Comput. Mol. Sci. **7**, e1322 (2017).

[53] K. Kitaura, E. Ikeo, T. Asada, T. Nakano, and M. Uebayasi, Chem. Phys. Lett. **313**, 701 (1999).

[54] Y. Inadomi, T. Nakano, K. Kitaura, and U. Nagashima, Chem. Phys. Lett. **364**, 139 (2002).

[55] S. Tsuneyuki, T. Kobori, K. Akagi, K. Sodeyama, K. Terakura, and H. Fukuyama, Chem. Phys. Lett. **476**, 104 (2009).

[56] D. G. Fedorov and K. Kitaura, J. Chem. Phys. **131**, 171106 (2009).

[57] D. G. Fedorov and K. Kitaura, J. Chem. Phys. **147**, 104106 (2017).

[58] J. Wen and H. Ma, Chem. Phys. Lett. **679**, 152 (2017).

[59] T. Fujita and Y. Mochizuki, J. Phys. Chem. A **122**, 3886 (2018).

[60] T. Kobori, K. Sodeyama, T. Otsuka, Y. Tateyama, and S. Tsuneyuki, J. Chem. Phys. **139**, 094113 (2013).

[61] H. Kitoh-Nishioka and K. Ando, Chem. Phys. Lett. **621**, 96 (2015).

[62] H. Kitoh-Nishioka and K. Ando, J. Chem. Phys. **145**, 114103 (2016).

[63] T. Fujita, Y. Haketa, H. Maeda, and T. Yamamoto, Org. Electron. **49**, 53 (2017).

[64] F. Aryasetiawan and O. Gunnarsson, Phys. Rev. B **49**, 16214 (1994).

[65] X. Blase and P. Ordejón, Phys. Rev. B **69**, 085111 (2004).

[66] X. Ren, P. Rinke, V. Blum, J. Wieferink, A. Tkatchenko, A. Sanfilippo, K. Reuter, and M. Scheffler, New J. Phys. **14**, 053020 (2012).

[67] K. Yasuda and D. Yamaki, J. Chem. Phys. **125**, 154101 (2006).

[68] C. Faber, P. Boulanger, C. Attaccalite, E. Cannuccia, I. Duchemin, T. Deutsch, and X. Blase, Phys. Rev. B **91**, 155109 (2015).

[69] F. Bruneval, N. Vast, and L. Reining, Phys. Rev. B **74**, 045102 (2006).

[70] M. Jain, J. Deslippe, G. Samsonidze, M. L. Cohen, J. R. Chelikowsky, and S. G. Louie, Phys. Rev. B **90**, 115148 (2014).

[71] Y. Okiyama, T. Nakano, K. Yamashita, Y. Mochizuki, N. Taguchi, and S. Tanaka, Chem. Phys. Lett. **490**, 84 (2010).

[72] T. Nakano, T. Kaminuma, T. Sato, Y. Akiyama, M. Uebayasi, and K. Kitaura, Chem. Phys. Lett. **351**, 475 (2002).

[73] V. Havu, V. Blum, P. Havu, and M. Scheffler, J. Comput. Phys. **228**, 8367 (2009).

[74] See Supplemental Material at http://link.aps.org/supplemental/10.1103/PhysRevB.98.205140 for additional information about the COHSEX and $G_0W_0$ results for the EHI and THI arrays, the MO self-energies in the pentacene thin film, and the details on the transfer integral calculations, which includes Refs. [75,76].

[75] B. Baumeier, J. Kirkpatrick, and D. Andrienko, Phys. Chem. Chem. Phys. **12**, 11103 (2010).

[76] P. Löwdin, J. Chem. Phys. **18**, 365 (1950).

[77] S. Schiefer, M. Huth, A. Dobrinevski, and B. Nickel, J. Am. Chem. Soc. **129**, 10316 (2007).

[78] M. J. Frisch, G. W. Trucks, H. B. Schlegel, G. E. Scuseria, M. A. Robb, J. R. Cheeseman, G. Scalmani, V. Barone, G. A. Petersson, H. Nakatsuji *et al.*, GAUSSIAN6 *Revision B.01* (2016), Gaussian Inc. Wallingford, CT.

[79] M. N. Bussac, J.-D. Picon, and L. Zuppiroli, Europhys. Lett. **66**, 392 (2004).

[80] S.-H. Ke, Phys. Rev. B **84**, 205415 (2011).

[81] F. Bruneval and M. A. L. Marques, J. Chem. Theory Comput. **9**, 324 (2013).

[82] J. Wilhelm, M. Del Ben, and J. Hutter, J. Chem. Theory Comput. **12**, 3623 (2016).

[83] D. G. Fedorov and K. Kitaura, J. Chem. Phys. **120**, 6832 (2004).